JOURNAL OF MATERIALS SCIENCE 31 (1996) 5885–5889

Molecular simulation of compressive failure in poly(*p*-phenylene teraphthalamide) crystals

D. J. LACKS
Department of Chemical Engineering, Tulane University, New Orleans, LA 70118 USA

Molecular mechanics simulations are carried out on crystals of poly(*p*-phenylene teraphthalamide) (PPTA) as a function of an applied axial compressive stress. The vibrational frequencies of the long wavelength acoustic modes which propagate along the chain axis and are polarized perpendicular to the plane of the hydrogen-bonded sheets are found to become imaginary when the imposed stress exceeds the modulus for shear between hydrogen-bonded sheets. The imaginary frequencies denote an elastic buckling instability. This instability occurs at a compressive stress of 0.3 GPa, in good agreement with the experimental result for the stress which causes material failure in PPTA fibres. It is suggested that previous overestimates of compressive strengths based on elastic buckling models occurred due to the use of the torsion modulus as the relevant shear modulus; however, the torsion modulus is not relevant because it represents an average of shear moduli in different directions, while elastic buckling takes place along the direction of easiest shear.

1. Introduction

Fibres composed of poly(*p*-phenylene teraphthalamide) (PPTA) are widely used in composite materials, under the trade name Kevlar®. These fibres have very good axial tensile strength, but their axial compressive strength is poor. The compressive strength is an order of magnitude less than the tensile strength [1], and compressive failure occurs at axial stresses of approximately 0.3 GPa [2]. Poor compressive properties are characteristic of many rigid-rod polymer fibres. The molecular origins of this compressive failure are not yet clear, due in part to the difficulty of carrying out experiments on the extremely narrow fibres.

Compressive failure in PPTA and other rigid-rod polymers has usually been attributed to a shear failure [2, 3, 4, 5]. The nature of the shear failure, however, is not well understood. DeTeresa *et al.* suggest that the failure is initiated by an elastic buckling instability, which is predicted to occur when the compressive stress exceeds the shear modulus [5]. Although experiments have demonstrated some correlation between compressive strengths and shear moduli of polymer fibres, compressive strengths are always found to be significantly lower than the shear moduli [6, 7]. Vlattas and Galiotis suggest that an inelastic shear instability precedes the elastic instability, to account for the compressive strength being lower than the shear modulus [2]. An inelastic instability, limited by the shear strength rather than the shear modulus, can arise from misorientations of the crystallites with respect to the fibre axis [8].

2. Computational method

Molecular simulations are carried out which focus on elastic instabilities in perfect crystals of PPTA. The effects of stress on the crystal structure are determined by minimizing the enthalpy (potential energy plus stress–strain energy) with respect to the atomic coordinates and lattice parameters. Elastic instabilities are detected from the stress dependence of the vibrational frequencies – an elastic instability occurs when the vibrational frequency of a mode decreases to zero and becomes imaginary (the vibrational frequencies depend on the crystal structure, and vary with stress due to changes in the structure with stress) [9]. An imaginary vibrational frequency implies that the atomic motion corresponding to that mode becomes non-oscillatory, and that the imposed crystal structure represents a saddle point rather than an energy minimum. The axial Young's modulus is obtained from the slope of the stress–strain curve, and the shear moduli are obtained from the appropriate second derivatives of the potential energy.

An infinite three-dimensional crystal is considered in the present simulations, and Ewald methods are used to evaluate the coulombic and dispersion energy sums [10]. Analytical first and second derivatives of the potential energy with respect to the atomic coordinates are calculated for use in geometry optimizations and the calculation of vibrational frequencies. Reciprocal-space (Brillouin zone) methods are used in the calculation of vibrational frequencies to allow the inclusion of long-wavelength vibrations [9]. The PCFF force field [11] is used for the potential energy surface.

0022–2461

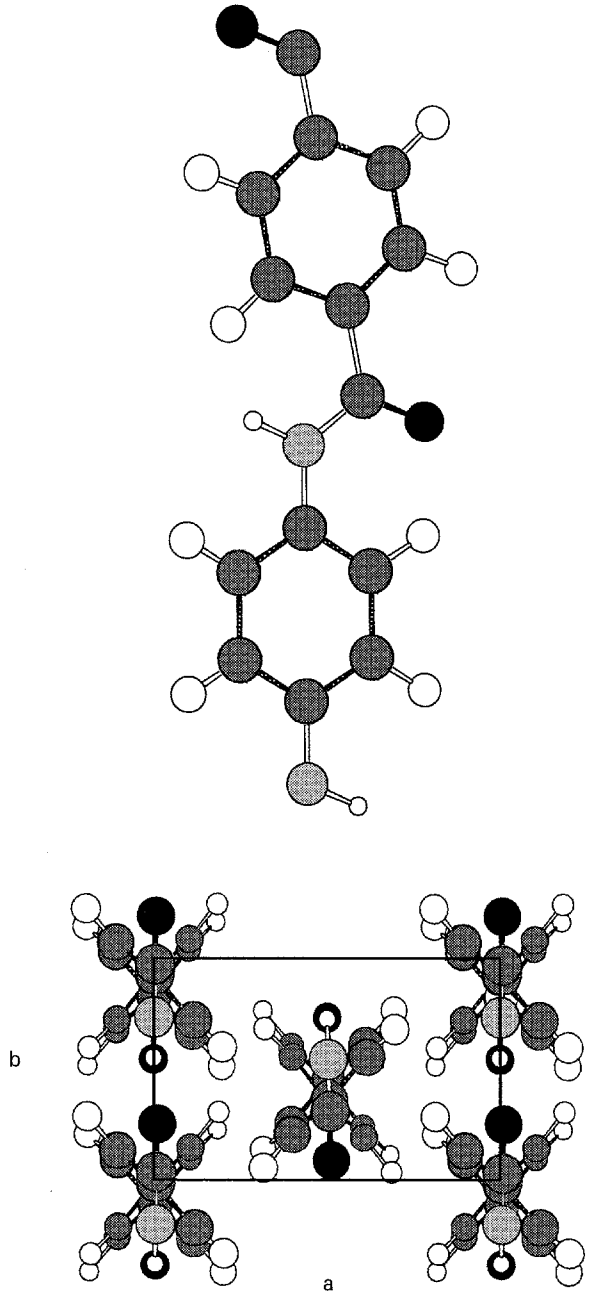

Figure 1 Monomer unit and crystal structure of PPTA. Key: carbon (black, backbone); hydrogen (white); oxygen (black, pendant); nitrogen (grey).

The crystal structure of PPTA, shown in Fig. 1, consists of hydrogen-bonded sheets parallel to the b–c plane. This aspect of the structure leads to significant anisotropy in the directions transverse to the chain axis – the forces along the b-axis are dominated by hydrogen bonding, and the forces along the a-axis are dominated by weaker dispersion interactions.

3. Results

The results for the structural parameters and relevant elastic parameters at zero stress are given in Table I. The structural parameters are in good agreement with the experimental values [12]. Although the elastic parameters do not agree as well with experiment, these results agree well with previous calculations [13]. Much of the overestimate of the axial Young's modulus in comparison with experiment [14] can be attributed to the neglect of thermal effects in the present calculation, which have been shown to significantly lower the calculated Young's modulus in PPTA [15]; these thermal effects would not affect the present conclusions, and are therefore not included in the present study. Some of the disagreement with the experimental Young's modulus is also likely to be due to experimental error: the difficulties in determining experimentally the ultimate properties of polymers are well known [16]. A detailed discussion of the calculated and experimental [6, 7, 17] shear moduli will be given below, but it is noted here that previous investigations have also found shear to be easier between hydrogen-bonded sheets (G_{ac}) than within the sheets (G_{bc}) [13, 18].

The vibrational frequencies of the transverse acoustic modes propagating along the chain axis, depicted schematically in Fig. 2, were calculated as a function of

TABLE I Structural parameters and relevant elastic moduli of PPTA at zero stress. Note that for shear, only one modulus is obtained experimentally (from torsion experiments)

	Simulation	Experiment
a (nm)	0.788	0.780[a]
b (nm)	0.513	0.519[a]
c (nm)	1.297	1.290[a]
γ(°)	90.75	90[a]
E_c (GPa)	311	240[b]
G_{bc} (GPa)	12.1	1.1[c], 1.2[d], 1.4[e], 1.9[f], 2.0[g]
G_{ac} (Gpa)	0.34	

[a] reference 12.
[b] extrapolation to complete chain orientation, reference 14.
[c] for Kevlar 149, reference 7.
[d] for Kevlar 49, reference 6.
[e] for Kevlar 49, reference 7.
[f] for Kevlar 29, reference 7.
[g] for Kevlar 49, reference 17.

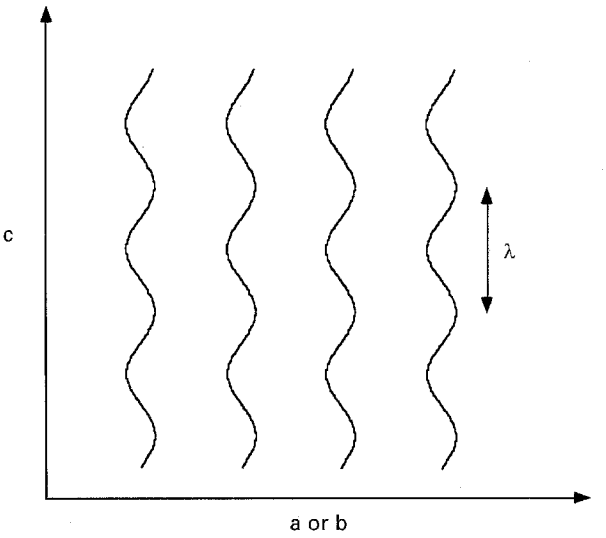

Figure 2 Schematic of the transverse acoustic vibrational modes which propagate along the chain axis. The lines represent polymer chains. The horizontal axis is the a-axis for modes polarized along the a-axis, and it is the b-axis for modes polarized along the b-axis. The wavevector k is related to the wavelength of vibration, λ, by $k = 2\pi/\lambda$.

the wavevector k. Axial compression has the effect of decreasing the frequencies of these vibrational modes. As shown in Fig. 3a, the frequencies of the long wavelength vibrations polarized along the a-axis decrease to zero and become imaginary for stresses between 0.3 GPa and 0.35 GPa (note that imaginary frequencies are displayed in Fig. 3 as negative). At a stress of 0.35 GPa the vibrations with wavelengths greater than 16.0 nm are unstable (the wavelength of a vibration is $2\pi/k$). These instabilities occur only along the a-axis (between hydrogen-bonded sheets), and as shown in Fig. 3b, the effects of compression are very minor for the vibrations polarized along the b-axis (within hydrogen-bonded sheets). This result agrees with experimental results which indicate that compression-induced shear deformation occurs only between hydrogen-bonded sheets [3].

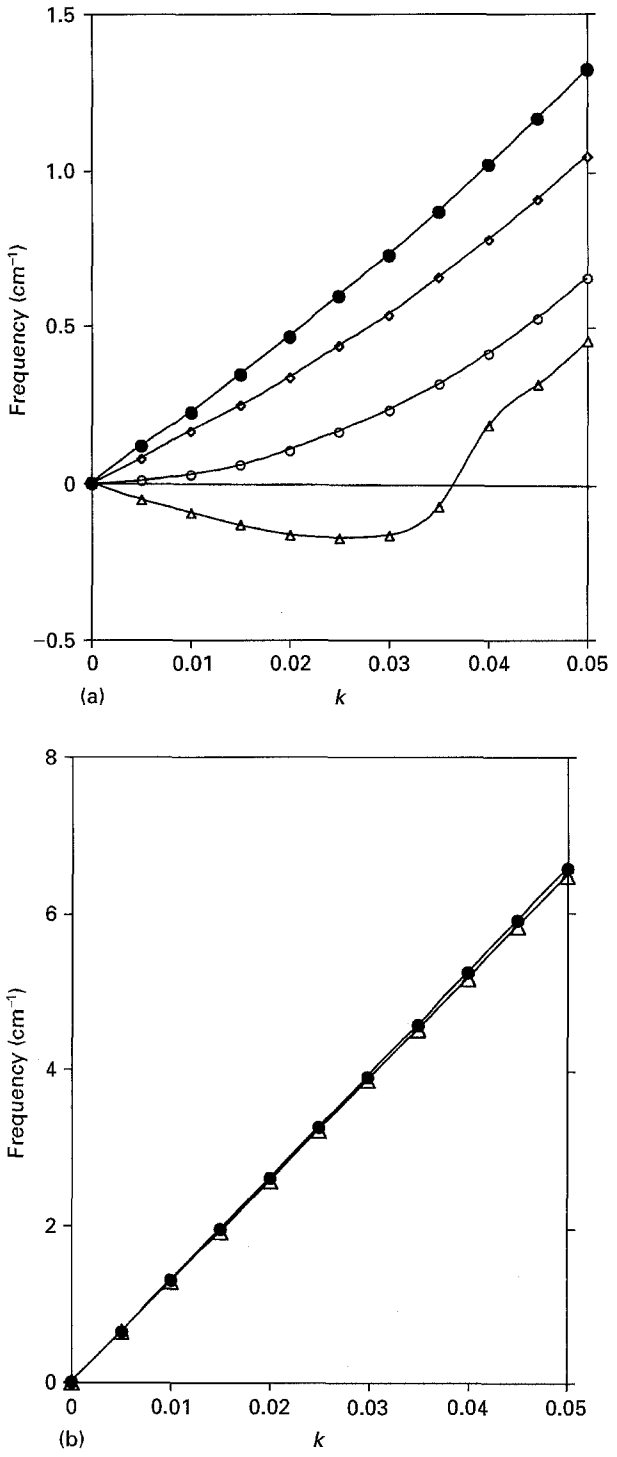

Figure 3 Vibrational frequencies for transverse acoustic modes which propagate along the chain axis, as a function of the wavevector k. (a) Modes polarized along the a-axis; (b) Modes polarized along the b-axis. Note that imaginary frequencies are displayed as negative. σ = (●) 0, (◇) 0.15, (○) 0.3, (△) 0.35 GPa.

These unstable vibrational modes signify that the zero-stress crystal structure becomes unstable at a compressive stress between 0.30 and 0.35 GPa. The new crystal structure will have a much larger unit cell along the chain axis. The stress at which the instability occurs is essentially equal to G_{ac}, the calculated modulus for shear between hydrogen-bonded sheets. Although the calculations were carried out on an infinite crystal, the results are relevant to finite crystallites because the wavelength of the unstable vibrations are smaller than the axial dimension of crystallites in PPTA fibres (approximately 80 nm) [19].

The elastic instability will be manifested in a deformation of the crystal structure corresponding to the atomic motion in the unstable vibrational modes (shown in Fig. 2). These deformations correspond exactly to the elastic buckling instabilities proposed by DeTeresa *et al.* [5]. Also, as proposed by DeTeresa *et al.*, this elastic instability occurs when the imposed stress exceeds the relevant shear modulus.

This elastic buckling mechanism differs from the bending deformation observed in previous molecular simulations of other rigid rod polymers at compressive strains of 2% [20]. Similar deformations were observed in the present PPTA simulations at stresses of approximately 3 GPa (which corresponds to strains slightly greater than 1%). The bending deformation corresponds to optical vibrational modes, and the molecular distortions occur identically in every monomer unit. In contrast, the elastic buckling instabilities correspond to long wavelength acoustic vibrational modes, where the molecular distortions are spread out over many monomer units. The elastic buckling instabilities consequently involve much smaller changes in bond angles and torsions and lead to smaller potential energy penalties, allowing them to occur at significantly lower compressive stresses. The elastic buckling instabilities correspond more closely to the long wavelength vibrational motions observed in previous single-chain molecular dynamics simulations [21].

4. Discussion

The present calculations predict compressive failure in PPTA crystals between 0.3 GPa and 0.35 GPa due to the elastic buckling mechanism proposed by DeTeresa *et al.*; this compressive strength is in very good agreement with the experimental result of approximately 0.3 GPa [2]. Such good agreement with experiment is at first surprising, since previous analyses of the elastic buckling model have concluded that the model leads to significant overestimates of the compressive strength [2, 5, 6]. These previous analyses have been based on shear moduli obtained from torsion experiments. It is proposed here that the torsion moduli are not the appropriate shear moduli to be used in regard

to the elastic buckling model – the elastic buckling will be limited by the direction of easiest shear (i.e. between hydrogen-bonded sheets), while the torsion modulus represents an average over shear in different directions.

Investigations of the morphology of PPTA fibres with electron diffraction techniques by Dobb *et al.* have shown that the fibres consist of radially oriented hydrogen bonded sheets, as shown schematically in Fig. 4a [22]. This radial orientation has been corroborated by optical microscopy and interference microscopy experiments [23, 24]. If this radial orientation is exact, the torsional modulus of the fibre, G, would correspond to G_{ac}, the shear modulus between hydrogen-bonded sheets [6]. However, NMR and X-ray diffraction experiments have indicated that the crystallites in PPTA are significantly smaller than 10 nm in the directions transverse to the chain axis [25, 26]; it seems likely that the many tiny crystallites will show a distribution of sheet orientations, rather than perfect radial orientation, as shown schematically in Fig. 4c. Based on an aggregate model [27], the torsional modulus of such an array of crystallites would correspond to an average of G_{ac} and G_{bc}

$$G = \int G_{ac} f(\vartheta) \cos^2 \vartheta \, d\vartheta + \int G_{bc} f(\vartheta) \sin^2 \vartheta \, d\vartheta \quad (1)$$

where $f(\vartheta)$ is the probability that a crystallite is oriented with its hydrogen-bonded sheets at an angle ϑ with the radial direction. It will be assumed that the crystallites show a Gaussian distribution of sheet orientations with respect to the radial direction

$$f(\vartheta) = (2\pi s)^{1/2} e^{-\vartheta^2/2s} \quad (2)$$

where s is the standard deviation of the angle of the hydrogen-bonded sheets from the radial direction. The resulting torsion modulus G, calculated with the G_{ac} and G_{bc} obtained from the present simulations, is shown in Fig. 5 as a function of s. These results show that standard deviations on the order of 15–25° account for the magnitudes of the observed torsion moduli in PPTA fibres (see Table I), and would explain the decrease in the torsional modulus in going from Kevlar 29 to Kevlar 49 to Kevlar 149 as being due to the increase in order observed in the fibres [26, 28] (the increase in order also manifests itself in the increase in values of the axial Young's modulus [2, 26]).

The present model for compressive failure in PPTA would account for the observation that the compressive strengths of Kevlar 29, Kevlar 49 and Kevlar 149 fibres are the same within experimental error [2]. Previous elastic buckling models, based on experimental torsion moduli, predict different compressive strengths for these fibres due to their different torsion moduli. Although the inelastic failure model can account for the compressive strengths of these fibres being the same, this model would require the cancellation of effects due to differences in axial crystallite misorientations with those due to differences in torsion moduli [2].

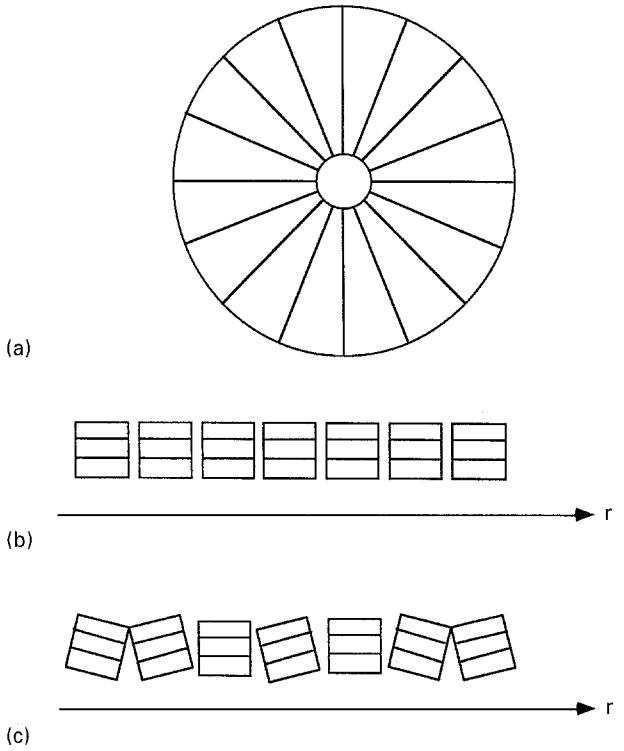

Figure 4 (a) Schematic of radial morphology in PPTA (view along fibre axis), after Dob *et al.* [22]; (b) Orientation of crystallites along radial direction assuming perfect radial orientation (view along fibre axis); (c) Orientation of crystallites assuming deviations from perfect radial orientation. Lines correspond to hydrogen-bonded sheets.

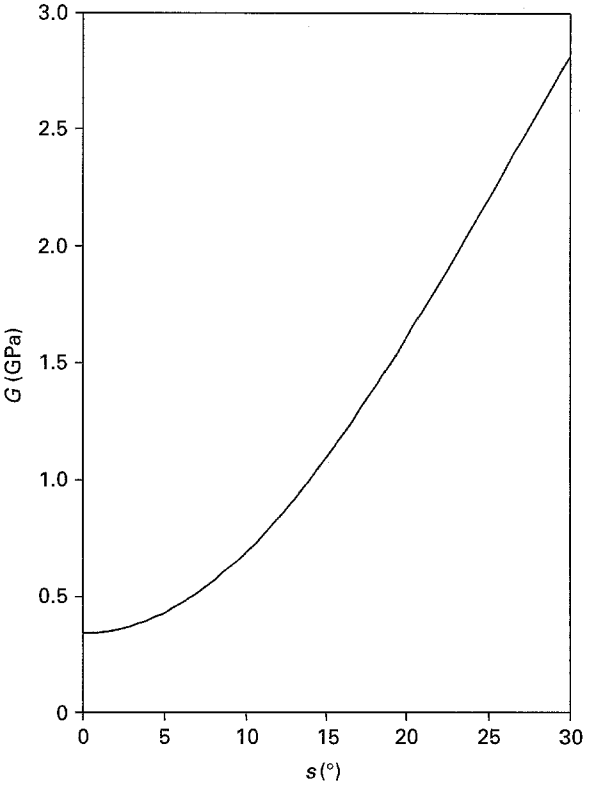

Figure 5 Torsion modulus of PPTA fibre calculated with the aggregate model and assuming approximate radial morphology. The values of G_{ac} and G_{bc} are taken from the present calculations, and it is assumed that the hydrogen-bonded sheets have a Gaussian distribution of orientations about the radial direction, with the distribution characterized by the standard deviation s.

The present model would also account for the observed linear relationship between the compressive strength and torsion modulus of a given fibre as a function of temperature [7]. This relationship would be expected from the present model if the crystallite orientations do not change with temperature, and the shear moduli G_{ac} and G_{bc} have similar temperature dependences.

5. Conclusions

Molecular simulations are carried out which suggest that the compressive failure in PPTA fibres arises from an elastic buckling instability which occurs when the compressive stress exceeds the shear modulus between hydrogen-bonded sheets. This mechanism is the same as that proposed by DeTeresa *et al.* [5]. Previous criticisms of this model were based on observations that compressive strengths were significantly lower than the shear moduli obtained from torsion experiments. However, the present results suggest that this overestimate occurs because the torsion modulus represents an average of shear moduli in different directions, whereas the elastic buckling will take place along the direction of easiest shear.

Acknowledgements

The author thanks the Louisiana Education Quality Support Fund for financial support.

References

1. J. M. GREENWOOD and P. G. ROSE, *J. Mater. Sci.* **9** (1974) 1809.
2. C. VLATTAS and C. GALIOTIS, *Polymer* **35** (1994) 2335.
3. T. TAKAHASHI, M. MIURA and K. SAKURAI, *J. Appl. Polym. Sci.* **28** (1983) 579.
4. D. C. MARTIN and E. L. THOMAS, *J. Mater. Sci.* **26** (1991) 5151.
5. S. J. DETERESA, R. S. PORTER and R. J. FARRIS, *ibid.* **20** (1985) 1645.
6. *Idem., ibid.* **23** (1988) 1886.
7. V. R. MEHTA and S. KUMAR, *ibid.* **29** (1994) 3658.
8. A. S. ARGON, in "Treatise on materials science and technology", edited by H. Herman, Vol. 1 (Academic Press, New York, 1972).
9. N. W. ASHCROFT and N. D. MERMIN, "Solid state physics" (Saunders College Press, Philadelphia, 1976).
10. N. KARASAWA and W. A. GODDARD, *J. Phys. Chem.* **93** (1989) 7320.
11. "Discover Software, version 2.3" (Biosym Technologies, San Diego, 1993).
12. H. TADOKORO, "Structure of crystalline polymers" (John Wiley & Sons, New York, 1979).
13. X. YANG and S. L. HSU, *Macromolecules* **24** (1991) 6680.
14. M. G. NORTHOLT, *Polymer* **21** (1980) 1199.
15. D. J. LACKS and G. C. RUTLEDGE, *Macromolecules* **27** (1994) 7197.
16. B. CRIST, *Annu. Rev. Mater. Sci.* **25** (1995) 295.
17. S. R. ALLEN, *Polymer* **29** (1988) 1091.
18. G. C. RUTLEDGE and U. W. SUTER, *Macromolecules* **24** (1991) 1921.
19. M. PANAR, P. AVAKIAN, R. C. BLUME, K. H. GARDNER, T. D. GIERKE and H. H. YANG, *J. Polym. Sci., Polym. Phys. Ed.* **21** (1983) 1955.
20. S. G. WIERSCHKE, J. R. SHOEMAKER, P. D. HAALAND, R. PACHTER and W. W. ADAMS, *Polymer* **33** (1992) 3357.
21. B. L. FARMER, B. R. CHAPMAN, D. S. DUDIS and W. W. ADAMS, *Polymer* **34** (1993) 1588.
22. M. G. DOBB, D. J. JOHNSON and B. P. SAVILLE, *J. Polym. Sci., Polym. Phys. Ed.* **15** (1977) 2201.
23. R. HAGEGE, M. JARRIN and M. SOTTON, *J. Microsc.* **115** (1978) 65.
24. S. B. WARNER, *Macromolecules* **16** (1983) 1546.
25. R. J. SCHADT, E. J. CAIN, K. H. GARDNER, V. GABARA, S. R. ALLEN and A. D. ENGLISH, *ibid.* **26** (1993) 6503.
26. M. G. DOBB and R. M. ROBSON, *J. Mater. Sci.* **25** (1990) 459.
27. I. M. WARD and D. W. HADLEY, "An introduction to the mechanical properties of solid polymers" (John Wiley & Sons, New York, 1993).
28. S. J. KRAUSE, D. L. VEZIE and W. W. ADAMS, *Polymer Comm.* **30** (1989) 10.

Received 16 February
and accepted 13 June 1996